Soft-Switching Boost Converter With a Flyback Snubber for High Power Applications

Tsai-Fu Wu, *Senior Member, IEEE*, Yong-Dong Chang, Chih-Hao Chang, and Jeng-Gung Yang

***Abstract*—This paper presents a soft-switching boost converter with a flyback snubber for high power applications. The proposed converter configuration can achieve both near zero-voltage and zero-current soft-switching features, while it can reduce the current and voltage stresses of the main switch. In this paper, several passive and active snubbers associated with boost converters are first reviewed, and their limitations are then addressed. One of the boost converters with a flyback snubber is proposed and analyzed in detail to explain the discussed features. Experimental results obtained from a 5-kW boost converter have confirmed that the proposed converter configuration is attractive and feasible for high power applications.**

***Index Terms*—Active snubber, boost converter, current stress, flyback snubber, passive snubber.**

I. Introduction

RENEWABLE energy resources have drawn a lot of attention. Photovoltaic (PV) energy is most popular as it is clean, maintenance free, and abundant. In order to obtain maximum power from PV modules, tracking the maximum power point of PV arrays is usually an essential part of a PV system, which is mostly realized with a boost converter.

For high power applications, component stress, switching loss, and electromagnetic interference noise are increased due to high di/dt of diode reverse-recovery current and high dv/dt of MOSFET drain–source voltage, resulting in low reliability and even violation of regulation. Hence, passive and active snubbers were introduced to the boost converter.

The extra snubber or commutation cell can create a short time interval of zero-voltage transition or zero current transition for the main switch to achieve a zero-voltage switching (ZVS) turn-ON or a zero-current switching (ZCS) turn-OFF process [1]–[3]. Passive snubbers are widely used in boost converter applications because they do not require many components and complex control, which can achieve soft-switching features [4]–[13]. To achieve near ZVS turn-ON soft-switching feature, an inductor is usually placed in series with the main switch or the diode to slow down diode reverse-recovery current. In these snubbers, although the inductor can alleviate reverse-recovery current, it induces extra voltage stress on the main switch at turn-OFF transition and would increase switching loss. Thus, a snubber capacitor is required to absorb the energy stored in the snubber inductor and to clamp the switch voltage. However, for saving component count, the energy stored in the snubber capacitor is recycled through the main switch, resulting in high current stress. It would deteriorate converter reliability and life span.

To release the aforementioned high current stress, active snubbers are applied to the boost converter [14]–[20]. They can not only attain soft-switching features, but significantly reduce voltage and current stresses. However, in the active snubber, its auxiliary switch needs to sustain at least the same current rating as that of the main switch because the input inductor current flows through the auxiliary switch during the main switch turn-OFF transition, reducing efficiency and reliability. In [20], the boost converter with a low voltage stress turn-ON snubber is integrated with an active snubber. It can improve high turn-OFF loss and achieve near ZCS turn-OFF and ZVS turn-ON soft-switching features for the main switch. However, its input and resonant currents will flow through the active snubber, resulting in high current stress on the auxiliary switch. Hence, to reduce the current rating of the auxiliary switch, a low power-rating flyback active snubber is introduced to the boost converter with a passive snubber. Additionally, it still can achieve near ZVS and near ZCS, and reduce current and voltage stresses imposed on the main switch.

In this paper, Section II reviews boost converters with passive and active snubbers. Section III presents the proposed converter configuration for reducing current and voltage stresses, while achieving near ZVS and ZCS soft-switching features. Section IV presents design procedure and practical consideration of the proposed converter. Experimental results obtained from a 5-kW prototype built with the proposed converter are presented in Section V to verify its feasibility. Finally, the paper is concluded in Section VI.

II. Review of the Boost Converter With Snubbers

Snubbers can either be passive or active networks. The basic function of a snubber is to absorb the energy from the parasitic devices in the power circuit to achieve soft-switching features. However, high voltage or high current stress still appears on the main switch. In the following, the main-switch soft-switching features with its voltage and current stresses will be discussed according to the snubber types of passive and active.

A. With Passive Snubbers

Fig. 1 shows a conventional boost converter and its conceptual switch gate signal, and voltage and current waveforms. It can be

Manuscript received July 12, 2010; revised November 25, 2010 and January 30, 2011; accepted March 4, 2011. Date of current version February 7, 2012. Recommended for publication by Associate Editor P. Barbosa.

The authors are with Elegant Power Application Research Center, Department of Electrical Engineering, National Chung Cheng University, Ming-Hsiung, Chia-Yi 621, Taiwan (e-mail: ieetfwu@ee.ccu.edu.tw).

Color versions of one or more of the figures in this paper are available online at http://ieeexplore.ieee.org.

Digital Object Identifier 10.1109/TPEL.2011.2126024

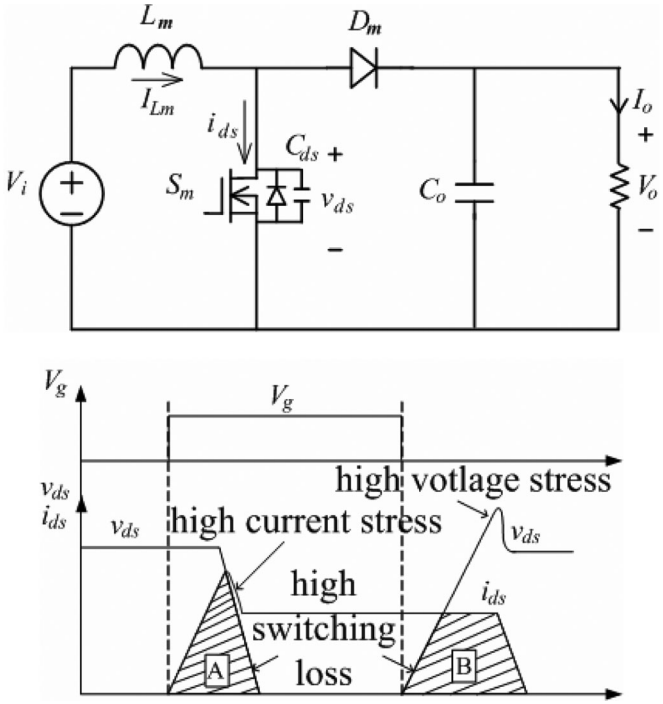

Fig. 1. Conventional boost converter.

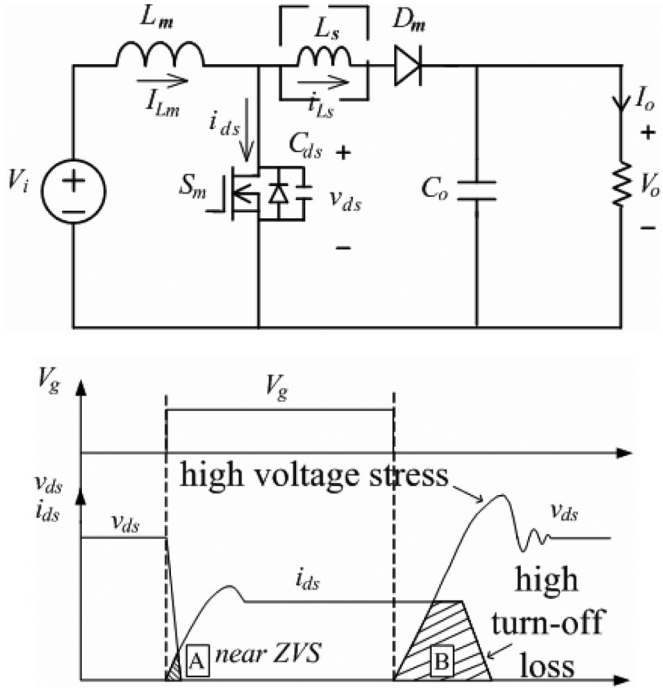

Fig. 2. Boost converter with a snubber inductor L_s.

observed that when the main switch is turned on, high current stress will occur, which is primarily due to the reverse-recovery current of diode D_m and input inductor current I_{Lm}. On the other hand, when the switch is turned off, high voltage stress will impose on the main switch caused by input voltage V_i, finite forward recovery time of D_m, and the ringing between parasitic devices. These will result in turn-ON and turn-OFF switching losses, as shown in areas A and B, respectively, and deterioration in conversion efficiency and reliability.

To achieve a turn-ON soft-switching feature, inserting an inductor in series with the main switch or diode is consequently adopted, as shown in Fig. 2. Inductor L_s can limit reverse-recovery current from diode D_m and share input inductor current flowing through main switch S_m during switching transition, achieving a near ZVS feature. Although turn-ON loss can be improved, part of inductor current will charge capacitor C_{ds} before $i_{Ls} = I_{Lm}$, resulting in high voltage stress imposed on the main switch.

For resolving the aforementioned problem, snubber capacitor C_s is added between components L_s and D_m, and two diodes D_1 and D_2 are used to clamp v_ds [4]–[6], as shown in Fig. 3. Note that L_s can be relocated to be in series with switch S_m. The reverse-recovery current in L_s creates the first resonant path of L_s–D_1–C_s to charge C_s through D_1. Even though the energy stored in C_s can help raise i_{Ls}, the main switch still turns off with hard-switching manner. Moreover, after C_s has been completely discharged, a large portion of current I_{Lm} will flow though diodes D_1 and D_2, increasing conduction loss a lot. Thus, efficiency and reliability of the converter have not been optimally improved yet.

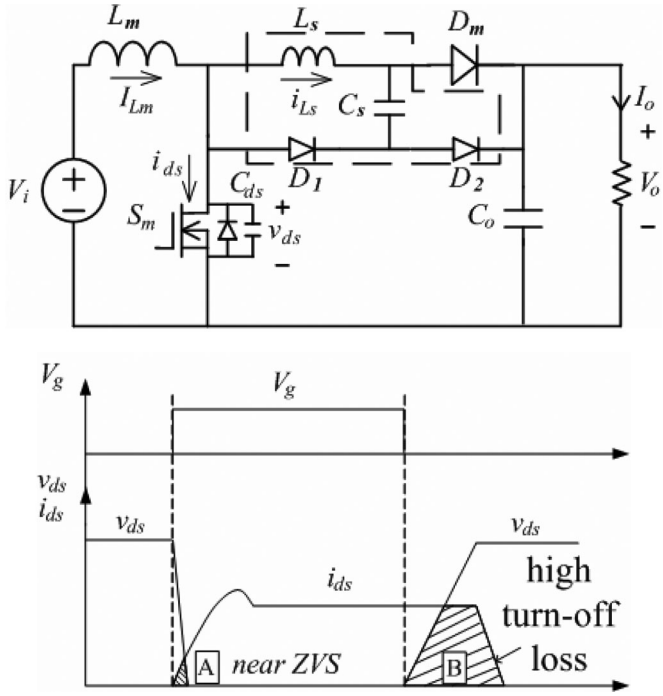

Fig. 3. Boost converter with a low voltage stress turn-ON snubber.

To achieve both near ZVS and ZCS, diode D_3, capacitors C_s and C_b, and coupled inductor L_a (for reducing conduction current through D_1, D_2, and D_3) are integrated in the snubber circuit [7]–[13], as shown in Fig. 4. In the circuit, the voltage of v_{Cb} can help reduce the start-up voltage level for exciting inductor L_s, which in turn will reduce the voltage stress of the

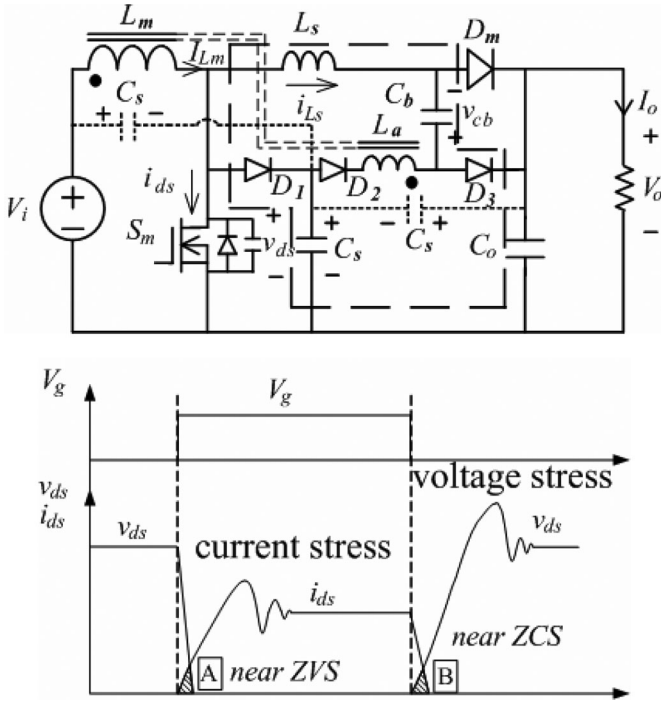

Fig. 4. Boost converter with a soft-switching turn-ON and turn-OFF snubber.

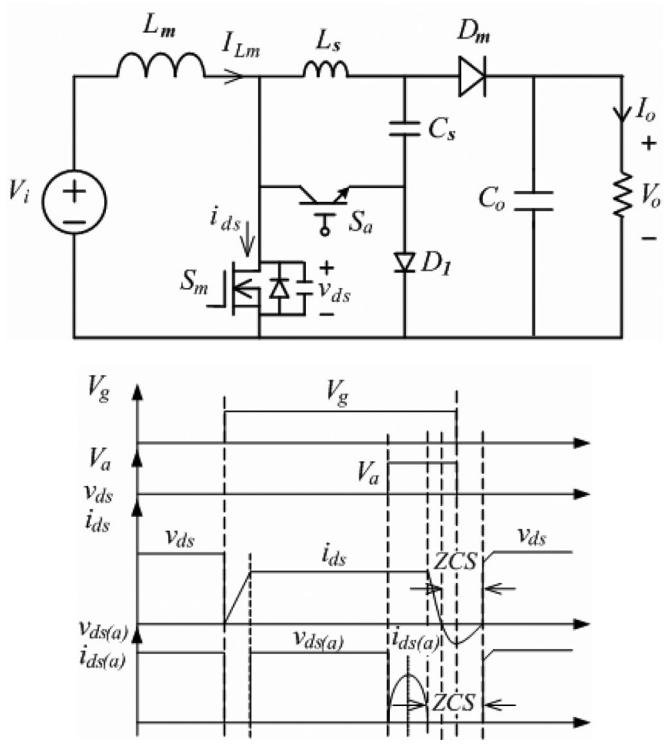

Fig. 5. Boost converter with a near ZVS turn-ON and ZCS turn-OFF active snubber.

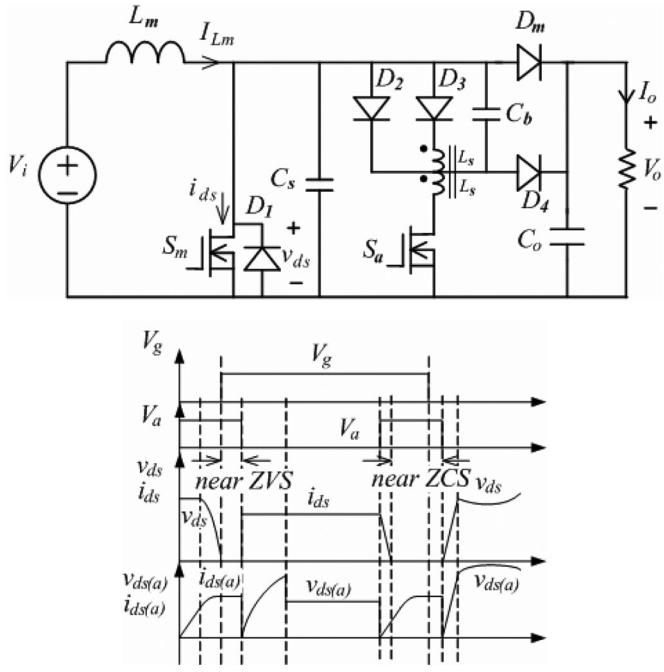

Fig. 6. Boost converter with a near ZVS and ZCS active snubber.

main switch. However, the discharging current of C_s still flows through the main switch, resulting in high current stress.

Due to less degrees of freedom, a boost converter with passive snubbers has the difficulty to achieve both near ZVS and ZCS, and also to keep low voltage and current spikes or stresses for the main switch. Thus, active snubbers were introduced to the boost converter.

B. With Active Snubbers

Nowadays, there has been a lot of study about various types of active snubbers to reduce either switching loss or voltage and current stress. In the literature, the examples that can achieve lower current stress imposed on the main switch with soft-switching features were proposed [14], [15], as shown in Figs. 5 and 6. The main advantage of the snubber is its simple structure, and it can achieve near ZVS and ZCS while with low voltage and current stresses imposed on the main switch. However, there typically exist three limitations: the auxiliary switch requiring a current rating as high as that of the main switch, high circulation loss during the snubber resonating stage, and sometimes it hard to control the auxiliary switch to meet the soft-switching condition under various input currents. Another variation version [16] of the ones shown in Figs. 5 and 6 is shown in Fig. 7, but it still comes out high current flowing through the auxiliary switch. Hence, this configuration is limited from high input current/high power applications.

III. Proposed Converter Configuration

Designing a snubber with high performance needs to consider various indexes of switching loss, current and voltage stresses, snubber circulation loss, duty loss, duty range, control complexity, component count, and processed power. In fact, there is no single passive or active snubber, which can meet all of the aforementioned performance considerations. This paper presents a boost converter with a low power-rating flyback active snubber for high input current/high power applications [21]. It can resolve the problems mentioned in Section II while it requires

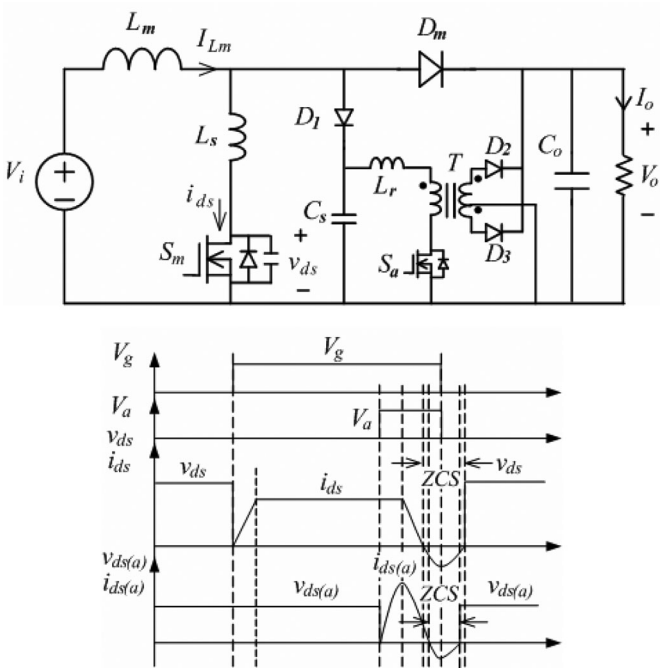

Fig. 7. Boost converter with an isolated near ZVS turn-ON and ZCS turn-OFF active snubber.

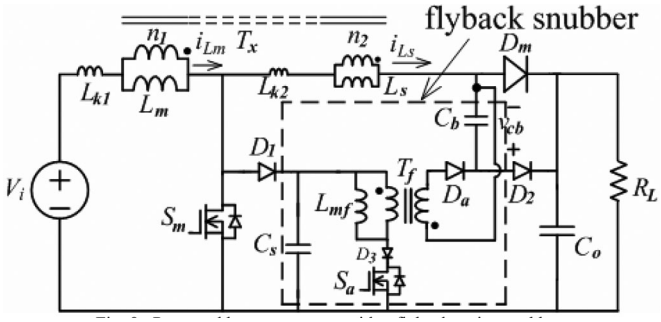

Fig. 8. Proposed boost converter with a flyback active snubber.

more component count. The proposed boost converter, as shown in Fig. 8, is formed with a main switch S_m, coupled inductors L_m and L_s, and a flyback snubber. In the circuit, L_{k1} and L_{k2} are the leakage inductance of coupled inductor T_x. The key current and voltage waveforms of the converter are shown in Fig. 9. Note that the proposed flyback snubber can be integrated with other pulsewidth modulation (PWM) converters, such as buck, buck-boost, and Cuk, to achieve the same soft-switching features.

In Fig. 8, clamp-branch diode D_1 and capacitor C_s can help achieve near ZCS for S_m. The energy stored in capacitor C_s does not circulate through main switch S_m while it is transferred to C_b through the flyback snubber, which is operated in discontinuous-conduction mode (DCM) to reduce switching loss and voltage stress. Buffer capacitor C_b plays the same role as the capacitor C_b shown in Fig. 4, and its stored energy is released to the output through diode D_2. The capacitor C_b not only buffers the energy transferred from C_s, but reduce voltage stress on S_m at turn-OFF transition.

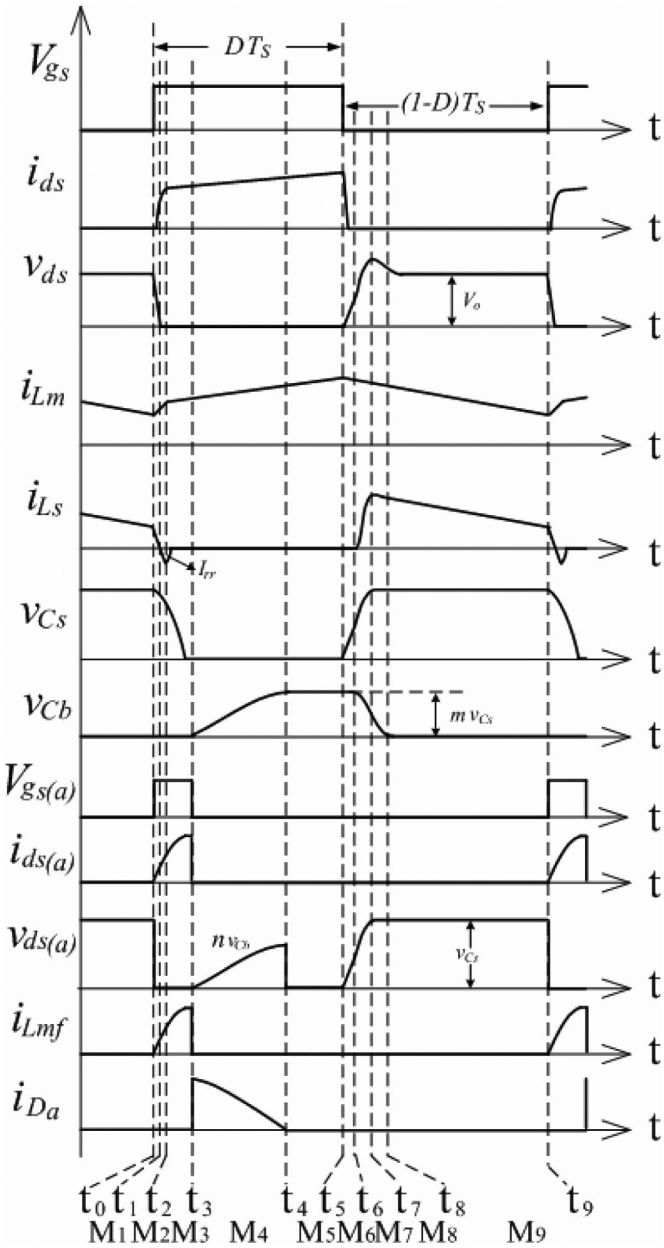

Fig. 9. Key current and voltage waveforms of the proposed converter.

To analyze the boost converter with a flyback active snubber, the following assumptions based on one switching cycle of the steady-state operation are made.

1) Both input voltage V_i and output voltage V_o are constant over one switching cycle.
2) Initial value of sunbber inductor L_s and capacitor C_s are equal to zero.
3) Capacitance of C_s is much greater than parasitic capacitance of the main switch; thus, parasitic capacitance can be ignored.
4) The efficiency of the flyback active snubber is 100%.

According to the aforementioned assumptions, operation of the proposed converter over one switching cycle can be divided into nine major operating modes. Fig. 10 shows the topological

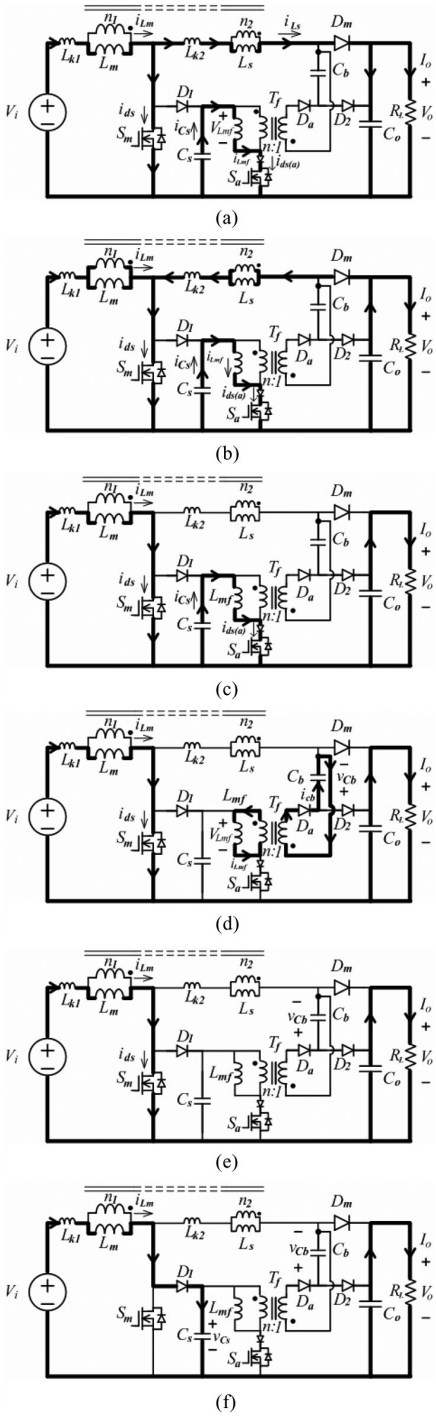

Fig. 10. Various circuit modes illustrating the operation of the boost converter with a flyback active snubber. (a) Mode 1 [$t_0 \le t < t_1$]. (b) Mode 2 [$t_1 \le t < t_2$]. (c) Mode 3 [$t_2 \le t < t_3$]. (d) Mode 4 [$t_3 \le t < t_4$]. (e) Mode 5 [$t_4 \le t < t_5$]. (f) Mode 6 [$t_5 \le t < t_6$]. (g) Mode 7 [$t_6 \le t < t_7$]. (h) Mode 8 [$t_7 \le t < t_8$]. (i) Mode 9 [$t_8 \le t < t_9$].

modes of the proposed converter, and each of which is explained as follows.

Mode 1 [Fig. 10(a), $t_0 \le t < t_1$]: Before t_0, main switch S_m was in the OFF state. The driving signals of both boost converter and flyback snubber are synchronously started at t_0.

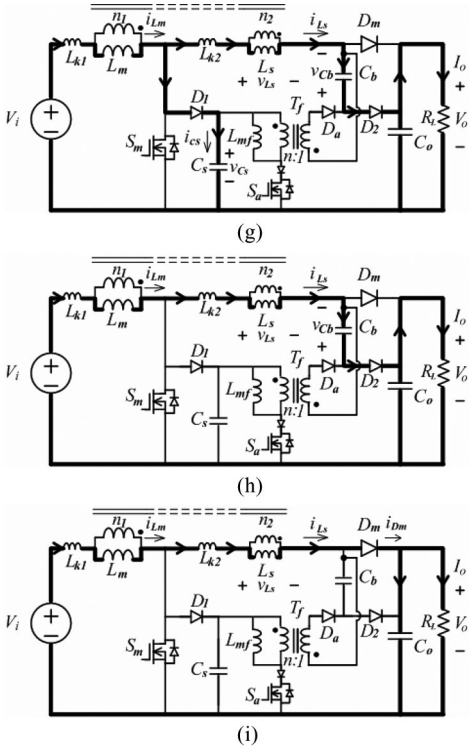

Fig. 10. *Continue*

In this mode, the boost converter achieves a near ZVS soft-switching feature, and current i_{Ls} drops to zero gradually.

In the flyback snubber, the energy stored in capacitor C_s will be delivered to magnetizing inductance $L_m f$, current $i_{Lm}f$ is therefore built up, and the equivalent circuit is shown in Fig. 10(a). During the energy-transfer process, both components C_s and $L_m f$ are in resonance. Currents $i_{Cs}(t)$, $i_{Lm}f(t)$, and $i_{ds}(f)(t)$ are identical; thus, current i_{Cs} *(t)* and voltage v_{Cs} *(t)* can be derived as follows:

$$i_{Cs}(t) = \frac{v_{Cs}(t_0)}{Z_0} \sin \omega_0 (t - t_0) \tag{1}$$

and

$$v_{Cs}(t) = v_{Cs}(t_0) \cos \omega_0 (t - t_0) \tag{2}$$

where the resonant frequency ω_0 and the characteristic impedance Z_0 are, respectively, expressed as follows:

$$\omega_0 = \frac{1}{\sqrt{L_{mf} C_s}} \tag{3}$$

and

$$Z_0 = \sqrt{\frac{L_{mf}}{C_s}}. \tag{4}$$

Since the flyback snubber is operated in DCM, the current and voltage rating of switch S_a are primarily determined by i_{Cs} and v_{Cs}. Moreover, since capacitor C_s can absorb the current difference between i_{Lm} and i_{Ls}, switch S_a does not need a current rating as high as that of S_m.

Mode 2 [Fig. 10(b), $t_1 \le t < t_2$]: Afterward, boost diode D_m is in reverse bias, and the equivalent circuit is shown in

Fig. 10(b). The *di*/*dt* of the boost diode reverse-recovery current is primarily limited by leakage inductance L_{k2}.

Mode 3 [Fig. 10(c), $t_2 \le t < t_3$]: In this mode, boost converter and flyback snubber are also maintained in the ON state. The energy from capacitor C_s is still delivered to magnetizing inductance L_{mf}. The equivalent circuit is shown in Fig. 10(c).

Mode 4 [Fig. 10(d), $t_3 \le t < t_4$]: When switch S_a is turned off at t_3, the energy stored in inductance L_{mf} starts to transfer to buffer capacitor C_b by way of D_a, and the equivalent circuit is shown in Fig. 10(d). During this interval, both magnetizing inductance L_{mf} and buffer capacitor C_b are in resonant manner; as a result, current i_{Cb} *(t)* and voltage v_{Cb} *(t)* can be derived as follows:

$$i_{Cb}(t) = I_{Lmf}(t_3)\cos\omega_3(t-t_3) + \frac{V_{Lmf}}{Z_3}\sin\omega_3(t-t_3) \tag{5}$$

and

$$v_{Cb}(t) = Z_3 I_{Lmf}(t_3)\sin\omega_3(t-t_3) - V_{Lmf}\cos\omega_3(t-t_3) \tag{6}$$

where $I_{Lm}f(t_3)$ is the initial current of magnetizing inductance L_{mf} at t_3, and resonant frequency ω_3 and characteristic impedance Z_3 can be determined as follows:

$$\omega_3 = \frac{1}{\sqrt{L_{mf}C_b}} \tag{7}$$

and

$$Z_3 = \sqrt{\frac{L_{mf}}{C_b}}. \tag{8}$$

Again, since the flyback snubber is operated in DCM, current i_{Cb} and voltage v_{Cb} will exclusively determine the ratings for diode D_a.

Mode 5 [Fig. 10(e), $t_4 \le t \le t_5$]: Because the energy stored in magnetizing inductance L_{mf} was completely transferred to capacitor C_b at t_4, currents $i_{ds(a)}$, i_{Lmf}, and i_{Da}, and voltage $v_{ds(a)}$ are equal to zero in this interval. Voltage v_{Cb} is clamped till time t_6. The equivalent circuit is shown in Fig. 10(e).

Mode 6 [Fig. 10(f), $t_5 \le t < t_6$]: This mode begins when the main switch S_m is turned off, and the snubber capacitor C_s is charged until its voltage is satisfied with the relationship shown in the following:

$$V_{Cs}(t_6) + V_{Cb}(t_6) = V_o \tag{9}$$

In this mode, the flyabck snubber still stays in the OFF state. The equivalent circuit is shown in Fig. 10(f).

Mode 7 [Fig. 10(g), $t_6 \le t < t_7$]: When (9) is satisfied, current i_{Ls} will start to track current i_{Lm} with a resonant manner, and capacitor C_b will start to release its stored energy. At time t_7, current i_{Ls} is equal to current i_{Lm}. Meanwhile, the voltage of the main switch S_m and capacitor C_s will reach the maximum value simultaneously, and an equivalent circuit is shown in Fig. 10(g). A near ZCS feature is therefore attained during t_5–t_7. In this mode, snubber capacitor C_s, equivalent inductance L_X ($= L_{k2} + L_s$), and buffer capacitor C_b are in resonance. Currents i_{Ls} *(t)* and i_{Cs} *(t)*, and voltages v_{Ls} *(t)*, v_{Cb} *(t)*, and v_{Cs} *(t)* can be derived as follows:

$$i_{Ls}(t) = \frac{C_X}{C_s} I_{Lm}[1-\cos\omega_6(t-t_6)] \tag{10}$$

$$i_{Cs}(t) = I_{Lm} - \frac{C_X}{C_s} I_{Lm}[1-\cos\omega_6(t-t_6)] \tag{11}$$

$$v_{Ls}(t) = \left(Z_6 I_{Lm}\frac{C_X}{C_s}\right)\sin\omega_6(t-t_6) \tag{12}$$

$$v_{Cb}(t) = \frac{I_{Lm}}{C_s+C_b}\left[\frac{1}{\omega_6}\sin\omega_6(t-t_6) - (t-t_6)\right] + V_{Cb}(t_6) \tag{13}$$

and

$$v_{Cs}(t) = \frac{1}{C_s}\left[I_{Lm}(t-t_6)\times\left(1-\frac{C_X}{C_s}\right) + \frac{C_X I_{Lm}}{C_s\omega_6}\sin\omega_6(t-t_6)\right] + V_{Cs}(t_6) \tag{14}$$

where $V_{Cb}(t_6)$ and $V_{Cs}(t_6)$ are the initial value of capacitors C_b and C_s at t_6, respectively, I_{Lm} is a constant value, and capacitor C_X, resonant frequency ω_6, and characteristic impedance Z_6 are, Respectively, expressed as follows:

$$C_X = \frac{C_s C_b}{C_s + C_b} \tag{15}$$

$$\omega_6 = \frac{1}{\sqrt{L_X C_X}} \tag{16}$$

$$Z_6 = \sqrt{\frac{L_X}{C_X}} \tag{17}$$

$$L_X = L_s + L_{k2}. \tag{18}$$

Mode 8 [Fig. 10(h), $t_7 \le t < t_8$]: Before t_8, the energy stored in buffer capacitor C_b was not completely drained out yet; thus, the capacitor will not stop discharging until its voltage drops to zero. The equivalent circuit is shown in Fig. 10(h). The energy stored in capacitor C_s is

$$W_{Cs} = \frac{1}{2}C_s \cdot v_{Cs}^2(t_7). \tag{19}$$

Based on the energy stored in capacitor C_s, we can determine the power rating P_f of the flyback snubber as follows:

$$P_f = W_{Cs} \cdot f_s \tag{20}$$

Under the conditions of $V_i = 200$ V and $P_{\max} = 5$ kW, voltage v_{Cs} can be determined from (14) as around 427 V; thus, the maximum power rating $P_{f(\max)}$ of the flyback snubber is just about 40 W. The processed power by the flyback snubber is less than 1% of the full power rating (5 kW).

Mode 9 [Fig. 10(i), $t_8 \le t < t_9$]: When the energy stored in C_b has been completely released to the output at t_8, diode D_m will conduct. In this interval, the voltage across the main switch will drop back to around output voltage V_o, and moreover, the circuit operation in this mode is identical to that of a conventional boost converter in the OFF state. The equivalent circuit is shown in Fig. 10(i). It should be noted that voltage v_{ds} might not be

higher than V_o under light-load condition and with a small L_s. A complete switching cycle ends at t_9.

IV. Design Procedure and Practical Consideration

This section presents the design of the power converter and selection of the major components. A brief design procedure is described as follows.

A. Design of the Boost Converter:

1) Main Switch (S_m): To operate the converter at a 5-kW power rating and 20-kHz switching frequency, the main switch can choose insulated gate bipolar transistor (IGBT), MOSFET, CoolMOS, or even better performance devices. UGenerally, IGBT devices are suitable for the main switch when the converter is designed for high power applications. Considering the effects of tail current, latchup, and negative temperature coefficient (most commercially available), the proposed converter does not use IGBT as the main switch, whereas a parallel connection of MOSFETs is adopted. In the experiment, two MOSFET IXFH36N50P with $R_{ds(\mathrm{on})} = 0.17\ \Omega$ were selected. In fact, it can be operated at higher switching frequency, but a time interval for the flyback snubber to transfer the energy from capacitors C_s to C_b has to be sustained.

2) Main Inductor (L_m): The main inductance of 1.2 mH was designed based on (21), which can be operated at continuous-conduction mode

$$L_m > L_B = \frac{V_o T_s}{2 I_{oB}} D(1-D)^2 \tag{21}$$

where L_B is the boundary inductance, T_s is the switching period, I_{oB} is the boundary output current, and D is the duty ratio.

In addition, core loss, saturation flux density, and frequency response of the inductor are also needed to be considered. Hence, according to the data sheet [22], two toroidal cores CH571125 in parallel are selected for the main inductor. The winding of two paralleled 18-AWG copper wires with 43 turns was designed.

3) Main Diode (D_m): The main diode contributes most of the loss in the converter. In considering fast reverse recovery, low forward voltage drop, and sufficient voltage rating, the boost diode is chosen with the rating of 600 V/60 A, DSEI 60-06A.

4) Output Capacitor (C_o): The output capacitor is used to buffer output voltage, suppress spikes, and filter ripple. It also needs to consider the entire load current under the full-load condition and system dynamic performance. Hence, three 470-μF electrolytic capacitors in parallel are adopted for output capacitor C_o.

B. Design of the Flyback Snubber

A flyback snubber is to transfer energy from snubber capacitor C_s to buffer capacitor C_b, which can attain near ZCS turn-OFF and ZVS turn-ON for main switch S_m. The key components of D_1, D_2, L_s, C_s, C_b, L_{mf}, S_a, D_3, and D_a are designed as follows.

TABLE I
Capacitance C_s Versus Voltage v_{Cs}

Capacitance C_s (nF)	Voltage v_{Cs} (V)
10	707
20	500
30	408

1) Clamping Diode (D_1) and Diode (D_2): Diodes D_1 and D_2 are placed at input and output of the flyback snubber. The task of D_1 is to block the current from C_s flowing through the main switch, and D_2 is to block output current I_o flowing to the flyback snubber. The 600-V/30-A rating of HFA30PA60C ultrafast soft recovery diode can be used for D_1. The voltage and current ratings of diode D_2 must be greater than output voltage V_o, and its average rectifier current should be greater than snubber inductor current i_{Ls}. Thus, diode D_2 can be chosen with the rating of 600 V/30 A HFA30PA60C.

2) Snubber Capacitor (C_s): Snubber capacitor C_s is to absorb current difference between currents i_{Lm} and i_{Ls}, which can attain near ZCS soft-switching feature for the main switch. Considering the processed power being around 1% of the full-load power and based on (19) and (20), the relationship between capacitance C_s and voltage v_{Cs} is shown in Table I. In practice, the capacitance of C_s is chosen as 22 nF.

3) Snubber Inductor and Capacitor set (L_s, C_s, and C_b): Design of snubber inductor L_s and capacitor set C_s and C_b can be achieved with MATLAB software package. In M_6 (see Fig. 9), current i_{Lm} flows through the low impedance-path capacitor C_s. Relationship among v_{Cs}, V_o, and v_{Cb} can be expressed as follows:when $v_{Cs} < V_o - V_{Cb}(t_6)$

$$i_{L_s} = 0 \qquad i_{C_s} = i_{L_m} \qquad C_s \frac{dv_{C_s}}{dt} = i_{C_s} \tag{22}$$

where $V_{Cb}(t_6)$is the initial value of v_{Cb}.

When capacitor C_s is charged to be high enough, it means that equation (9) is satisfied, and the converter enters M_7 operation. Current i_{Lm} will flow through the path of L_{k2}–L_s–C_b–D_2–C_o with a resonant manner, which creates a near ZCS operational opportunity for main switch S_m. The following relationship can be obtained:when $v_{Cs} \geq V_o - V_{Cb}(t_6)$

$$C_s \frac{dv_{C_s}}{dt} = i_{C_s} \qquad L_s \frac{di_{L_s}}{dt} = v_{C_s} - (V_o - v_{C_b})$$
$$C_b \frac{dv_{C_b}}{dt} = i_{C_b} \qquad i_{C_s} = i_{L_m} - i_{L_s}. \tag{23}$$

Based on the aforementioned conditions, snubber inductance L_s, processed power of the flyback snubber, capacitor set C_s and C_b, and voltage v_{Cs} and v_{Cb} can be derived. It can be proved that higher snubber inductance L_s can reduce diode reverse-recovery loss, whereas the flyback snubber needs to process higher power and higher voltage will cross the snubber capacitor, resulting in lower conversion efficiency. In considering voltage stress on switch S_m, circulation loss, turn-OFF loss, and design margin, a proper capacitor set of $C_s = 22$ nF and $C_b = 47$ nF is chosen for the proposed converter. Coupled inductor L_s and its leakage inductance are used to limit the reverse-recovery current of diode D_m. It is chosen as $L_s = 2.5\ \mu$H to limit the current effectively.

4) Magnetizing Inductance (L_{mf}): The magnetic device in the flyback snubber plays the role of a transformer and a coupled inductor, resulting in high leakage inductance. To reduce high voltage spike occurring on switch S_a due to the leakage inductance, the flyback snubber is usually operated in DCM. Thus, magnetizing inductance L_{mf} should satisfy the following inequality:

$$L_{mf} < L_{mfB} = \frac{n^2(v_{Cb} + V_{F(Df)})}{2I_{oB}}(1-D)^2 T_s \qquad (24)$$

where $L_{mf}B$ is the boundary inductance, and I_{oB} is the boundary output current. When choosing turns ratio $n = 1$, $I_{oB} = 4$ A, $D = 0.2$, and $T_s = 50$ μs, based on (25) (v_{Cb} can be determined as 292 V), and from datasheet ($V_F(Da) = 1.28$ V), magnetizing inductance L_{mf} can be determined as 1.17 mH. Here, the value of 1 mH is adopted.

5) Switch (S_a) and Blocking Diode (D_3): To choose a proper switching device for S_a, its current and voltage stresses should be determined first. The current and voltage stress can be determined as follows:

$$i_{ds(a),\text{peak}} = \frac{v_{Cs}}{\sqrt{L_{mf}/C_s}} \qquad (25)$$

and

$$v_{ds(a)} = Max(nv_{Cb} + v_{Cs}, v_{Cs}) \qquad (26)$$

Initially, $v_{Cb} = 0$, and finally, $v_{Cs} = 0$, and since $n = 1$, $v_{ds(a)} = v_{Cs}$. The peak current can be calculated as around 2 A, and the voltage stress can be calculated as around 430 V. Hence, switch S_a is chosen with the rating of 500 V/8 A, IRF840 MOSFET. In addition, blocking diode D_3 has the same voltage rating as that of switch S_a; thus, the diode can be chosen as an ultrafast rectifier MUR450 with the rating of 500 V/4 A.

6) Diode (D_a): Diode D_a in the flyback snubber was also operated under DCM condition. Its current stress can be also determined from (25), while its voltage stress can be determined as follows:

$$v_{Da} \geq \frac{v_{Cs}}{n} + v_{Cb} \qquad (27)$$

Initially, $v_{Cb} = 0$, and since $n = 1$, $v_{Da} = v_{Cs} = v_{ds(a)}$. Thus, diode D_a can be also chosen as an MUR450.

V. Experimental Results

To verify the proposed converter performance, an experimental prototype of 5-kW boost converter with a flyback snubber was designed and built, as shown in Fig. 11, and its specifications are listed as follows:

1) input voltage V_i : 100–250 V_{dc};
2) input current I_i : 25 A at $V_i = 200$ V;
3) switching frequency f_s : 20 kHz;
4) output voltage V_o : 360 $\pm$ 20V_{dc};
5) output power : $P_{o(\max)} = 5$ kW at $V_i = 200$ V.

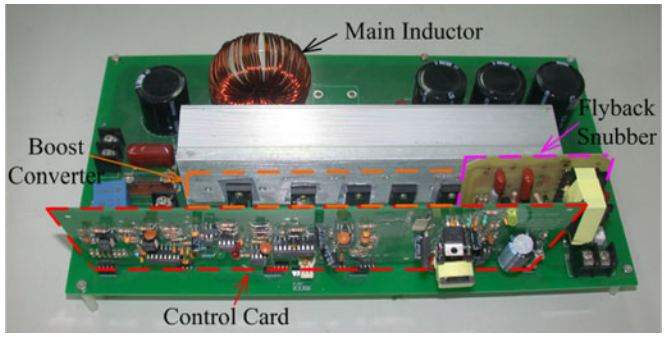

Fig. 11. Photograph of the prototype converter.

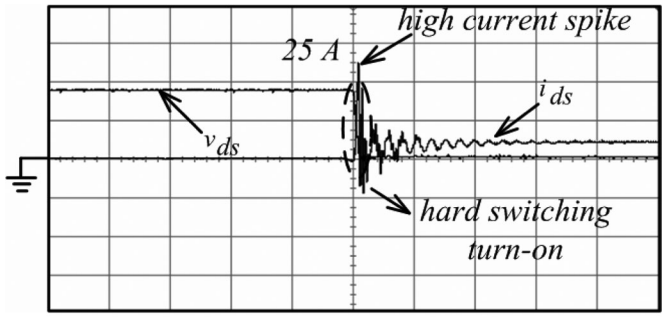

(200 V/div, 10 A/div, 0.5μ s/div)

(a)

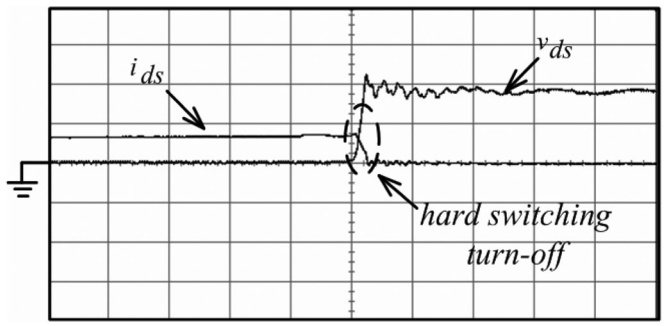

(200 V/div, 10 A /div, 0.5μ s/div)

(b)

Fig. 12. Measured voltage v_{ds} and current i_{ds} waveforms of main switch S_m at (a) turn-ON and (b) turn-OFF transitions from the conventional boost converter under 1-kW load condition. (a) (200 V/div, 10 A/div, 0.5 μs/div), (b) (200 V/div, 10 A /div, 0.5 μs/div).

From the aforementioned specifications, the key components can be determined as follows:

1) main switch S_m: IXFH36N50P $*$ 2;
2) main diode D_m : DSEI 60-06A ;
3) diode D_1 : HFA30PA60C;
4) diode D_2 : HFA30PA60C;
5) diode D_3 : MUR450;
6) diode D_a : MUR450;
7) auxiliary switch S_a : IRF840;
8) T_f core : 3C90 / EI-35;
9) main core : CH571125 $*$ 2;
10) main inductor L_m : 1.2 mH;
11) coupled inductance L_s : 2.5 μH;
12) inductor L_{mf} : 1 mH;

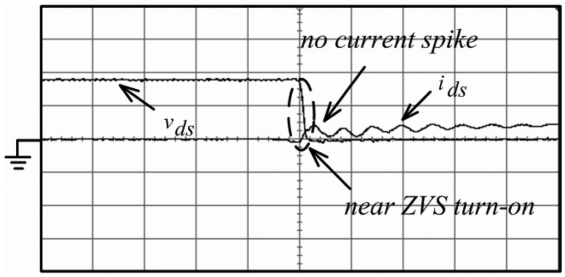

(200 V/div, 10 A/div, 0.5μ s/div)

(a)

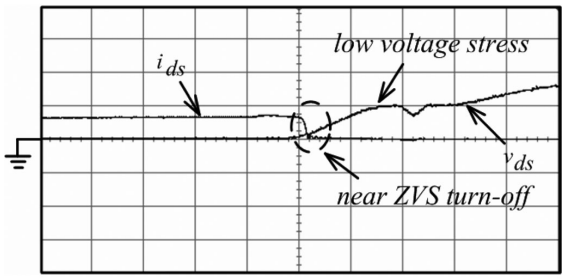

(200 V/div, 10 A /div, 0.5μ s/div)

(b)

Fig. 13. Measured voltage v_{ds} and current i_{ds} waveforms of main switch S_m at (a) turn-ON and (b) turn-OFF transitions from the proposed boost converter with a flyback snubber and under 1-kW load condition. (a) (200 V/div, 10 A/div, 0.5 μs/div). (b) (200 V/div, 10 A /div, 0.5 μs/div).

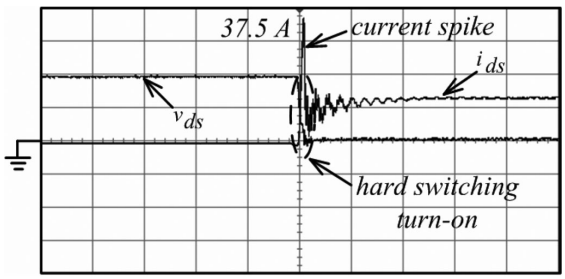

(200 V/div, 10 A/div, 0.5μ s/div)

(a)

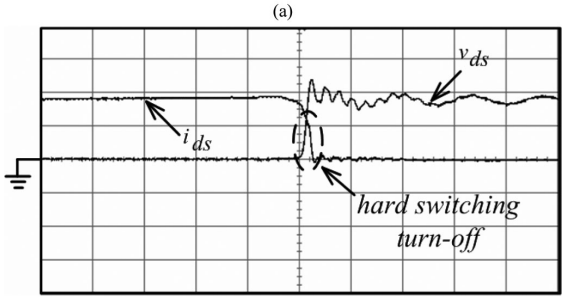

(200 V/div, 10 A /div, 0.5μ s/div)

(b)

Fig. 14. Measured voltage v_{ds} and current i_{ds} waveforms of main switch S_m at (a) turn-ON and (b) turn-OFF transitions from the conventional boost converter under 3-kW load condition. (a) (200 V/div, 10 A/div, 0.5 μs/div). (b) (200 V/div, 10 A /div, 0.5 μs/div).

13) snubber capacitance C_s : 22 nF;
14) capacitor C_b : 47 nF;
15) capacitor C_o : 470 $*$ 3μF.

The proposed boost converter is compared with a conventional one under various load conditions. Measured voltage v_{ds} and current i_{ds} waveforms from the converters operated under 1-kW load condition are shown in Figs. 12 and 13, respectively. From Fig. 12, it can be observed that operation of a conventional boost converter will result in loss at turn-ON and turn-OFF transitions. While from Fig. 13, a boost converter with a flyback snubber can result in no current spike, low voltage stress, and less switching loss at turn-ON and turn-OFF transitions.

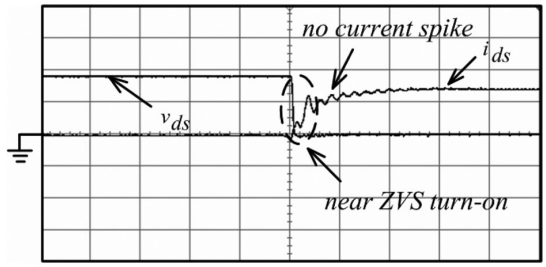

(200 V/div, 10 A/div, 0.5μ s/div)

(a)

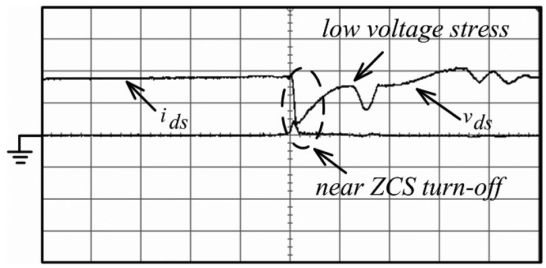

(200 V/div, 10 A /div, 0.5μ s/div)

(b)

Fig. 15. Measured voltage v_{ds} and current i_{ds} waveforms of main switch S_m at (a) turn-on and (b) turn-off transitions from the proposed boost converter with a flyback snubber and under 3 kW load condition. (a) (200 V/div, 10 A/div, 0.5 μs/div) (b) (200 V/div, 10 A /div, 0.5 μs/div)

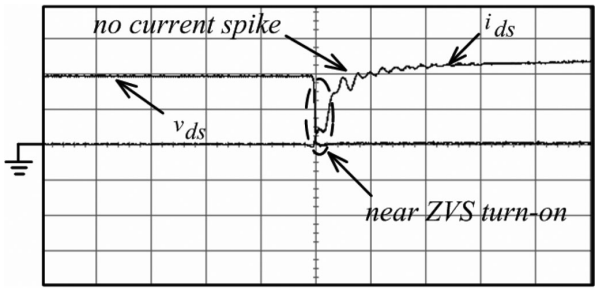

(200 V/div, 10 A/div, 0.5μ s/div)

(a)

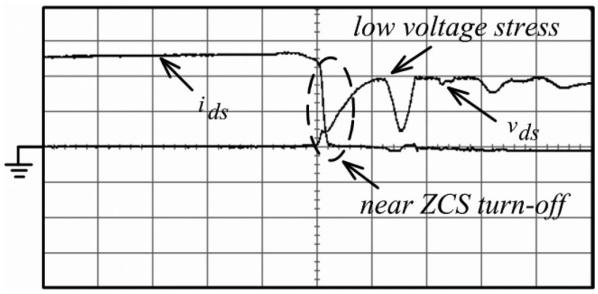

(200 V/div, 10 A /div, 0.5μ s/div)

(b)

Fig. 16. Measured voltage v_{ds} and current i_{ds} waveforms of main switch S_m at (a) turn-on and (b) turn-off transitions from the proposed boost converter with a flyback snubber and under the full load condition (5 kW). (a) (200 V/div, 10 A/div, 0.5 μs/div), (b) (200 V/div, 10 A /div, 0.5 μs/div).

TABLE II
POWER LOSS ESTIMATION OF THE KEY COMPONENT IN THE CONVERTER

Part	Type/Value	Power loss estimation
S_m	IXFH36N50P*2	$P_{CON}^{Main} = 2\times(\frac{i_{ds}}{2})^2 \times R_{ds(on)} \times D = 2\times(\frac{25}{2})^2 \times 0.17 \times 0.45 = 23.9$ W, $P_{on}^{Main} = 2\times\frac{1}{2}\times C_{ds}\cdot V_o^2 \times f_s = 2\times\frac{1}{2}\times(470\times10^{-12})\cdot 360^2\times(20\times10^3)$ $= 1.22$ W (due to C_{ds}), and $P_{loss}^{Sm} = 23.9 + 1.22 = 25.12$ W.
Coupled inductors	L_m =1.2 mH L_s = 2.5 μH (CH571125)	$B = \frac{V_{Lm}\times DT_s}{N\times A_e}\times10^8 = \frac{200\times0.45\times50\mu s}{86\times2.29}\times10^8 = 2285$ G, $P_L = 600\ mW/cm^3$, (obtained from its datasheet) $P_{core}^{Coup} = P_L \times V_e = 600(mW/cm^3)\times28.6(cm^3) = 17.16$ W, $P_{copper}^{Lm} = i_{Lm}^2 R_{Coup}^{Lm} = 25^2\times70.21\times10^{-3} = 43.88$ W, $P_{copper}^{Ls} = i_{Ls}^2 R_{Coup}^{Ls} = 25^2\times7.2\times10^{-3} = 4.5$ W and $P_{loss}^{ind} = P_{core}^{Coup} + P_{copper}^{Lm} + P_{copper}^{Ls} = 17.16 + 43.88 + 4.5 = 65.54$ W.
D_m	DSEI 60-06A	$P_{Dm} = i_{Dm}\times V_F \times (1-D) = 25\times1.6\times0.55 = 22$ W.

Figs. 14 and 15 show those waveforms under 3-kW load condition. Again, operation of a conventional boost converter comes out with high current spike (37.5 A), high voltage stress, and high switching loss, as shown in Fig. 14, while Fig. 15 shows that near ZVS and ZCS soft-switching features can be achieved with the proposed converter. When the power rating goes higher than 3 kW, the conventional boost converter does not work properly. Under the full-load condition (5 kW), measured current and voltage waveforms of main switch S_m in the proposed boost converter with a flyback snubber at turn-ON and turn-OFF transitions are shown in Fig. 16(a) and (b), respectively. From Fig. 16(a), it can be seen that reverse-recovery current and current stress can be well limited. From Fig. 16(b), it can be observed that high voltage stress can be further suppressed. Both near ZVS turn-ON and ZCS turn-OFF can be attained by the proposed converter under various load conditions.

Power loss of the proposed boost converter with a flyback snubber under 5-kW power rating is estimated to verify the measured efficiency. The key component types/values of the experimental converter and the power loss estimation are listed in Table II [23]. In addition to the aforementioned key component power loss estimation, other power losses include the auxiliary device power loss, near ZCS switching loss of the main switch, equivalent series resistance of the capacitors, trace losses, etc., which are around 20 W. Finally, the estimated total power loss and efficiency of the proposed boost converter with a flyback snubber can be summarized as follows:

$$P_{\text{loss}}^{\text{Total}} = P_{\text{loss}}^{\text{Sm}} + P_{\text{loss}}^{\text{ind}} + P_{\text{loss}}^{\text{Dm}} + P_{\text{loss}}^{\text{flyback}} + P_{\text{loss}}^{\text{others}} = 25.12 + 65.54 + 22 + 4 + 20 = 136.66\ \text{W} \quad (28)$$

and the conversion efficiency is

$$\eta^{\text{Total}} = \frac{P_i - P_{\text{loss}}^{\text{Total}}}{P_i} = \frac{5000 - 136.66}{5000} = 97.26. \quad (29)$$

Fig. 17 shows plots of the efficiency versus output power from 1 to 5 kW of the proposed boost converter with a flyback snubber. From the plots, we can see that the proposed converter can achieve over 97% conversion efficiency under 5-kW power rating, which is relatively consistent with the estimation. Even though the proposed converter with a flyback snubber only improves around 1% efficiency, as compared with that of a conventional converter, high current and voltage stresses have been suppressed by the flyback snubber. The converter reliability and life span can be therefore significantly improved. Additionally, the highest power loss is dissipated in the main core based on the estimation listed in Table II. When using a small core (CH571125), the highest efficiency occurs at 2 kW. Due to core and copper losses, the efficiency drops when the load condition goes beyond 2 kW. To improve the efficiency, the core of CH571125 is replaced by larger sizes of CH610125 and CH778060, and the wire of 18 AWG is replaced by 16 and 13 AWG. The efficiency measurements are also shown in Fig. 17. With CH610125 magnetic core, the efficiency is obviously increased, but the maximum efficiency is still occurring around 2 kW. By adopting CH778060 magnetic core, the maximum efficiency has been already shifted to 3 kW. These tests reveal that the efficiency drop at higher power level is primarily due to conduction loss. UMoreover, the efficiency measurement from the converter with IGBT switch (HGTG40N60A4) is also shown in Fig. 17. It can be seen that the converter with MOSFET still yields higher efficiency than that with IGBT, while it requires two MOSFETs. UThus, to design a converter with higher efficiency, it requires to reduce conduction loss in copper and even switches.

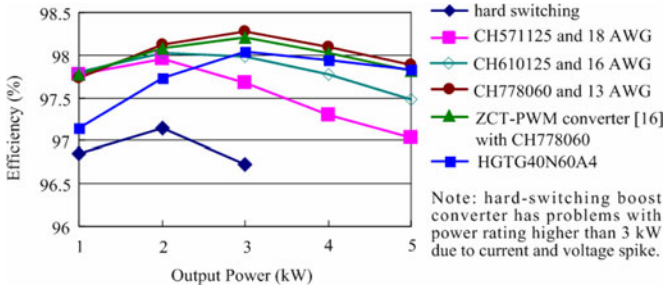

Fig. 17. Plots of efficiency versus output power.

In addition, performances of a boost converter with the passive and the active snubbers mentioned in Section II are compared, as summarized in Tables III and IV, respectively. From Table III, we can see clearly that both turn-ON and turn-OFF switching features, and both low current and low voltage

TABLE III
COMPARISON AMONG THE PERFORMANCES OF A BOOST CONVERTER WITH PASSIVE SNUBBERS

Type of snubbers / Performance Index	Without snubber	With a snubber inductor L_s (see Fig. 2)	With a low voltage stress turn-on snubber [5] (see Fig. 3)	With a soft switching turn-on and -off snubber [10] (see Fig. 4)
soft switching feature of S_m	● hard switching	● near ZVS turn-on	● near ZVS turn-on	● near ZVS turn-on ● near ZCS turn-off
switching loss to S_m	● high turn-on and -off losses	● high turn-off loss	● high turn-off loss	● low turn-on and -off losses
current and voltage stresses	● high spike current due to I_{rr} ● medium voltage stress due to t_{fr} $v_{ds(peak)} = I_{Lm} \times \sqrt{(L_m / C_{ds})}$	● spike current limited by L_s ● high voltage stress $v_{ds(peak)} = I_{Lm} \times \sqrt{L_s / C_{ds}}$	● spike current limited by L_s ● low voltage stress (clamped to V_o)	● high current stress $i_{ds(peak)} = I_{Lm} + \frac{v_{Cs}}{\sqrt{L_s (C_s + C_b) / C_s C_b}}$ ● low voltage stress (clamped to V_o)
snubber circulation loss	● no circulation current	● no circulation current	● low	● high (caused by C_s, C_b and L_s in resonance)
duty loss	● no	● low (caused only by L_s)	● medium (caused by L_s and C_s in resonance)	● high (caused by C_s, C_b and L_s in resonance)
duty range	● no limitation	● requiring a minimum turn-off time	● requiring a minimum turn-off time	● requiring a minimum turn-on time
component count	● no extra component	● 1 inductor	● 1 inductor ● 1 capacitor ● 2 diodes	● 2 inductors ● 2 capacitors ● 3 diodes

Note: 1. I_{rr} denotes the reverse recovery current of diode D_m.
2. t_{fr} denotes the forward recovery time of diode D_m.

TABLE IV
COMPARISON AMONG THE PERFORMANCES OF A BOOST CONVERTER WITH ACTIVE SNUBBERS

Type of snubbers / Performance Index	With a near ZVS turn-on and ZCS turn-off active snubber[14] (see Fig. 5)	With a near ZVS and ZCS active snubber [15] (see Fig. 6)	With an isolated near ZVS turn-on and ZCS turn-off active snubber [16] (see Fig. 7)	With a flyback active snubber (proposed)
soft switching feature of S_m	● near ZVS turn-on ● ZCS turn-off	● near ZVS turn-on ● near ZCS turn-off	● near ZVS turn-on ● ZCS turn-off	● near ZVS turn-on ● near ZCS turn-off
soft switching feature of S_a	● near ZVS turn-on ● ZCS turn-off	● near ZVS turn-on ● near ZCS turn-off	● near ZVS turn-on ● ZCS turn-off	● near ZVS turn-on ● ZCS turn-off (operated in DCM)
current and voltage stresses on S_m	● low current stress (I_{Lm}) ● low voltage stress (V_o)	● low current stress (I_{Lm}) ● low voltage stress (V_o)	● low current stress (I_{Lm}) ● low voltage stress (V_o)	● low current stress (I_{Lm}) ● low voltage stress (V_o)
current and voltage stresses on S_a	● high current stress $i_{ds(a)(peak)} = V_o / \sqrt{(L_r / C_r)} \geq I_{Lm}$ ● low voltage stress (V_o)	● high current stress $i_{ds(a)(peak)} = I_{Lm} + \sqrt{I_{rr}^2 + [V_o / (L_s / C_b)]}$ ● high voltage stress $v_{ds(a)(peak)} = V_o + I_{Lm} \cdot \sqrt{(L_s / C_b)}$	● high current stress $i_{ds(a)(peak)} = I_{Lm} + \frac{v_{Cr}}{\sqrt{(L_r / C_r)}}$ ● low voltage stress (V_o)	● low current stress (I_{Lm}) ● low voltage stress (V_o)
snubber circulation loss	● high (resonant current)	● high (twice circulation current in one switch cycle)	● high (input current and resonant current)	● low (due to flyback converter only)
control principle for S_a	● S_a turn-off is synchronized with S_m.	● S_a needs to switch on and off twice during S_m on-state	● *switch* S_a needs to conduct input current plus the resonant current of L_r-C_r for half a resonant period	● S_a is synchronously turned on with S_m.
duty loss	● caused by L_s and C_s	● caused by L_s and C_s at S_m turn-on transition ● caused by L_s and C_b during S_m on-state	● caused by L_s at S_m turn-on transition ● caused by L_r and C_s during S_m on-state	● caused by L_s at S_m turn-on transition ● caused by C_b and L_s at S_m turn-off transition
duty range	● turn-on period of S_m must be longer than that of S_a	● turn-on and turn-off periods of S_m must be longer than that of S_a	● turn-on period of S_m must be longer than that of S_a	● turn-on period of S_m must be longer than that of S_a
component count	● 1 inductor ● 1 capacitor ● 1 diode ● 1 active switch	● 2 inductors ● 1 capacitor ● 4 diodes ● 1 active switch	● 2 inductors ● 1 capacitor ● 3 diodes ● 1 transformer ● 1 active switch	● 1 inductor ● 2 capacitors ● 4 diodes ● 1 transformer ● 1 active switch

stress cannot be achieved simultaneously with passive snubbers. To achieve both soft-switching features, more component count is usually required. Besides, circulation current is inevitable when there exist *LC* components in the snubber. From Table IV, it can be seen that the active sunbbers can suppress current spike/stress, and achieve near ZVS turn-ON and ZCS, or near ZCS turn-OFF features. However, using resonant technique would cause additional current/voltage stresses imposed on the auxiliary switch. As a result, the auxiliary switch requires a current rating as high as that of the main switch. Also, the resonant technique would induce extra duty loss at S_m turn-ON and turn-OFF transitions, and snubber circulation loss is correspondingly increased. Although the proposed flyback active snubber does not need high switch current rating, it requires more component count.

VI. CONCLUSION

In this paper, a 5-kW boost converter with a flyback snubber has been implemented to verify its feasibility. Theoretical analysis and design procedure have been presented in detail, and the performance of boost converters with passive and active snubbers have been compared according to various indexes. Experimental results have shown that low current stress and near ZVS feature at main switch turn-ON transition have been attained, and low voltage stress and near ZCS feature at turn-OFF transition have been also achieved. As compared with the conventional boost converter, the proposed converter can achieve the highest efficiency, around 98% at 3-kW output power, while sustain low current and low voltage stresses. The maximum efficiency point can be shifted to a higher power level by

introducing larger core and lower copper wire gauge, which can reduce conduction loss. A boost converter with the proposed flyback snubber is relatively suitable for high power applications. Moreover, the proposed flyback snubber can be integrated with other PWM converters to achieve soft-switching feature and low component stress.

REFERENCES

[1] I. Aksoy, H. Bodur, and A. F. Bakan, "A new ZVT-ZCT-PWM DC-DC converter," *IEEE Trans. Power Electron.*, vol. 25, no. 8, pp. 2093–2105, Aug. 2010.

[2] C. M. de Oliveira Stein and H. L. Hey, "A true ZCZVT commutation cell for PWM converters," *IEEE Trans. Power Electron.*, vol. 15, no. 1, pp. 185–193, Jan. 2000.

[3] C. M. de Oliveira Stein, H. A. Grundling, H. Pinheiro, J. R. Pinheiro, and H. L. Hey, "Zero-current and zero-voltage soft-transition commutation cell for PWM inverters," *IEEE Trans. Power Electron.*, vol. 19, no. 2, pp. 396–403, Mar. 2004.

[4] R. Garcia, R. Liu, and V. Lee, "Optimal design for natural convection-cooled rectifiers," in *Proc. IEEE 18th Int. Telecommun. Energy Conf.*, 1996, vol. 2, pp. 813–822.

[5] C.-L. Chen and C.-J. Tseng, "Passive lossless snubbers for DC/DC converters," in *Proc. IEE Circuits, Devices Syst.*, 1998, vol. 145, no. 6, pp. 396–401.

[6] T. Irving and M. M. Jovanovic, "Analysis, design, and performance evaluation of flying-capacitor passive lossless snubber applied to PFC boost converter," in *Proc. IEEE Appl. Power Electron. Conf.*, vol. 1, pp. 503–508, 2002.

[7] N.-H. Kutkut, "Investigation of soft switched IGBT based boost converters for high power applications," in *Proc. Ind. Appl. Conf.*, 1997, vol. 2, pp. 1616–1623.

[8] C.-J. Tseng and C.-L. Chen, "A passive lossless snubber cell for non-isolated PWM DC/DC converters," *IEEE Trans. Ind. Electron.*, vol. 45, no. 4, pp. 593–601, Aug. 1998.

[9] X. Wu, X. Jin, L. Huang, and G. Feng, "A lossless snubber for DC/DC converter and its application in PFC," in *Proc. IEEE Int. Power Electron. Motion Control Conf.*, 2000, vol. 3, pp. 1144–1149.

[10] Z. Lin and K. Dong, "A novel of passive soft-switching with charge-pump snubber," in *Proc. IEEE Power Electron. Motion Control Conf.*, 2004, vol. 1, pp. 121–125.

[11] F. K. A. Lima, C. M. T. Cruz, and F. L. M. Antunes, "A family of turn-on and turn-off non-dissipative passive snubbers for soft-switching single-phase rectifier with reduced conduction losses," in *Proc. IEEE Appl. Power Electron. Conf.*, 2004, vol. 5, pp. 3745–3750.

[12] R. T. H. Li, H.S.-H. Chung, and A.K.T. Sung *IEEE Trans. Power Electron.*, vol. 25, no. 3, pp. 602–613, Mar. 2010.

[13] R. T. H. Li and H.S.-H. Chung, "A passive lossless snubber cell with minimum stress and wide soft-switching range," *IEEE Trans. Power Electron.*, vol. 25, no. 7, pp. 1725–1738, Jul. 2010.

[14] D.-Y. Lee, M.-K. Lee, D.-S. Hyun, and I. Choy, "New zero-current-transition PWM DC/DC converters without current stress," *IEEE Trans. Power Electron.*, vol. 18, no. 1, pp. 95–104, Jan. 2003.

[15] H. Bodur and A. F. Bakan, "A new near ZVS-ZCT-PWM DC-DC converter," *IEEE Trans. Power Electron.*, vol. 19, no. 3, pp. 676–684, 2004.

[16] P. Das and G. Moschopoulos, "A comparative study of zero-current-transition PWM converters," *IEEE Trans. Ind. Electron.*, vol. 54, no. 3, pp. 1319–1328, Jun. 2007.

[17] T.-F Wu, C.-C. Chen, C.-L Shen, and C.-N. Wu, "Analysis, design, and practical considerations for 500 W power factor correctors," *IEEE Trans. Aerosp. Electron. Syst.*, vol. 39, no. 3, pp. 961–975, Jul. 2003.

[18] H.-S. Choi and B. H. Cho, "Novel zero-current-switching (ZCS) PWM switch cell minimizing additional conduction loss," *IEEE Trans. Ind. Electron.*, vol. 49, no. 1, pp. 165–172, Feb. 2002.

[19] R. Liu, "Comparative study of snubber circuits for DC-DC converters utilized in high power off-line power supply applications," in *Proc. IEEE Appl. Power Electron. Conf.*, 1999, vol. 2, pp. 821–826.

[20] R. Streit and D. Tollik, "High efficiency telecom rectifier using a novel soft-switched boost-based input current shaper," in *Proc. Int. Telecommun. Energy Conf.*, 1991, pp. 720–726.

[21] T.-F. Wu, Y.-C. Chen, J.-G. Yang, and C.-L. Kuo, "Isolated bidirectional full-bridge DC–DC converter with a flyback snubber," *IEEE Trans. Power Electron.*, vol. 25, no. 7, pp. 1915–1922, 2010.

[22] *High Flux Magnetic Core CH571125 Datasheet*. Changsung Corp., Incheon, Korea. (2011). [Online]. Available: http://eng.changsung. com/.

[23] T.-F. Wu, C.-T. Tsai, Y.-D. Chang, and Y.-M. Chen, "Analysis and implementation of an improved current-doubler rectifier with coupled inductors," *IEEE Trans. Power Electron.*, vol. 23, no. 6, pp. 2681–2693, Nov. 2008.

Tsai-Fu Wu (S'88–M'91–SM'98) received the B.S. degree in electronic engineering from the National Chiao-Tung University, Hsinchu, Taiwan, in 1983, the M.S. degree in electrical and computer engineering from Ohio University, Athens, in 1988, and the Ph.D. degree in electrical engineering and computer science from the University of Illinois, Chicago, in 1992.

From 1985 to 1986, he was a System Engineer at SAMPO, Inc., Taipei, Taiwan, where he was engaged in developing and designing graphic terminals. From 1988 to 1992, he was a Teaching and Research Assistant in the Department of Electrical Engineering and Computer Science, University of Illinois, Chicago. Since 1993, he has been with the Department of Electrical Engineering, National Chung Cheng University, Chia-Yi, Taiwan, where he is currently a Chair Professor and the Director of the Elegant Power Application Research Center. His current research interests include developing and modeling of power converters, design of electronic dimming ballasts for fluorescent lamps, metal halide lamps and plasma display panels, design of solar-array supplied inverters for grid connection, and design of pulsed-electrical-field generators for transdermal drug delivery and food pasteurization.

Prof. Wu received three Best Paper Awards from Taipei Power Electronics Association in 2003–2005. In 2006, he was awarded as an Outstanding Researcher by the National Science Council, Taiwan. He is a Senior Member of the Chinese Institute of Engineers.

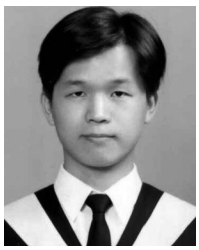

Yong-Dong Chang was born in Taiwan, in 1975. He received the B.S. and M.S. degrees in electrical engineering from Kun Shan University, Tainan, Taiwan, in 2002 and 2004, respectively. He is currently working toward the Ph.D. degree in the Department of Electrical Engineering, National Chung Cheng University, Chia-Yi.

His current research interests include the design and implementation of resonant converters for battery chargers, pulsed voltage generator application for liquid food sterilization, and investigation of soft-switching feature for high power converter applications.

Chih-Hao Chang is currently working toward the Ph.D. degree at Elegant Power Application Research Center, National Chung Cheng University, Chia-Yi, Taiwan.

His current research interests include three-phase grid-connected inverter, three-phase power factor correction, and dc microgrid.

Jeng-Gung Yang was born in Taiwan, in 1985. He received the B.S. degree in electrical engineering from National Chung Cheng University, Chia-Yi, Taiwan, in 2009 where he is currently working toward the M.S. degree.

His research interests include the design and development of soft-switching power converters.